AGU PUBLICATIONS

Water Resources Research

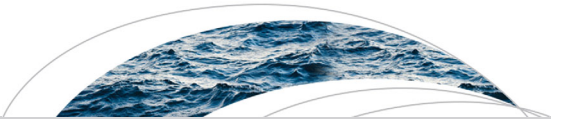

RESEARCH ARTICLE

10.1002/2013WR014506

Key Points:
- Precipitation is variable and uniform precipitation gradients cannot be derived
- Temperature lapse rates are not constant throughout the year and shallow
- Temperature lapse rates and precipitation gradients are key inputs in modeling

Correspondence to:
W. W. Immerzeel,
w.w.immerzeel@uu.nl

Citation:
Immerzeel, W. W., L. Petersen, S. Ragettli, and F. Pellicciotti (2014), The importance of observed gradients of air temperature and precipitation for modeling runoff from a glacierized watershed in the Nepalese Himalayas, *Water Resour. Res.*, *50*, doi:10.1002/2013WR014506.

Received 1 AUG 2013
Accepted 17 JAN 2014
Accepted article online 22 JAN 2014

The importance of observed gradients of air temperature and precipitation for modeling runoff from a glacierized watershed in the Nepalese Himalayas

W. W. Immerzeel[1,2,3], L. Petersen[2], S. Ragettli[2], and F. Pellicciotti[2]

[1]Department of Physical Geography, Utrecht University, Utrecht, Netherlands, [2]Hydrology and Water Resources Management, Institute of Environmental Engineering, ETH Zurich, Zurich, Switzerland, [3]International Centre for Integrated Mountain Development, Kathmandu, Nepal

Abstract The performance of glaciohydrological models which simulate catchment response to climate variability depends to a large degree on the data used to force the models. The forcing data become increasingly important in high-elevation, glacierized catchments where the interplay between extreme topography, climate, and the cryosphere is complex. It is challenging to generate a reliable forcing data set that captures this spatial heterogeneity. In this paper, we analyze the results of a 1 year field campaign focusing on air temperature and precipitation observations in the Langtang valley in the Nepalese Himalayas. We use the observed time series to characterize both temperature lapse rates (LRs) and precipitation gradients (PGs). We study their spatial and temporal variability, and we attempt to identify possible controlling factors. We show that very clear LRs exist in the valley and that there are strong seasonal differences related to the water vapor content in the atmosphere. Results also show that the LRs are generally shallower than the commonly used environmental lapse rates. The analysis of the precipitation observations reveals that there is great variability in precipitation over short horizontal distances. A uniform valley wide PG cannot be established, and several scale-dependent mechanisms may explain our observations. We complete our analysis by showing the impact of the observed LRs and PGs on the outputs of the TOPKAPI-ETH glaciohydrological model. We conclude that LRs and PGs have a very large impact on the water balance composition and that short-term monitoring campaigns have the potential to improve model quality considerably.

1. Introduction

The Himalayas and Tibetan plateau form the source areas of Asia's major river systems, yet their hydrology is poorly understood due to inaccessibility, the large variation in climates over short horizontal distances, and the absence of observations [*Immerzeel et al*., 2010]. Hydrological modeling is a challenging task in such environments, as the availability of hydrometeorological data sets at high altitude is extremely limited, a high model resolution is required to account for the large spatiotemporal variability of climate and physiography, and many key processes such as orographic precipitation and glacier melt under debris-covered glaciers are poorly understood [*Viviroli et al*., 2011; *Ragettli et al*., 2013a]. Little is known about the variability in space and time of climate drivers such as temperature and precipitation in these high-elevation catchments with extreme topography. For this reason simple approaches have been used to distribute point observations in space to create gridded input to spatially distributed models [*Tahir et al*., 2011; *Immerzeel et al*., 2012b]. As a result, the major challenge in such studies is dealing with internal processes, e.g., an underestimation of precipitation can be compensated in the model by an overestimation of melt [*Pellicciotti et al*., 2012]. Yet well-targeted field campaigns, even of short duration, have the potential to overcome these challenges [*Pellicciotti et al*., 2012; *Ragettli and Pellicciotti*, 2012].

In the Nepalese Himalayas several precipitation mechanisms can be distinguished as a result of large-scale circulation in combination with mesoscale orographical and thermal induced circulation [*Ueno and Yamada*, 1990]. Depending on the mechanism, the altitude dependence may also vary. *Seko* [1987] hypothesized that at the large scale, the monsoon season from June to September is the dominant mechanism, and that during the monsoon the total precipitation amount decreases from Kathmandu (1400 m) upward. *Bookhagen and Burbank* [2006] confirm this, and they show a strong relationship with the topography and

monsoon rainfall. Their work shows that there are two topography-related zones of high rainfall: one at around 1200 m elevation and a second one at 2100 m. At higher elevation the precipitation (at a larger scale) gradually decreases with elevation.

However, at the valley-scale convective precipitation occurs, which is associated with thermal circulation in the valley, and the precipitation near 5300 m was significantly higher than at 3800 m. This contradicts with the large-scale hypothesis of a negative relation between elevation and precipitation [*Ueno and Yamada*, 1990].

During winter, precipitation is produced by synoptic disturbances from the west. Westerly troughs develop over the west side of the Tibetan plateau and move eastward along the southern periphery of the plateau. Associated with the intrusion of troughs is a warm southerly moist air flow, bringing precipitation in the Himalaya which is amplified at high altitude. Winter precipitation generally occurs on a limited number of days, but the daily amounts can be considerable [*Seko*, 1987; *Shiraiwa et al*., 1992; *Steinegger et al*., 1993].

Air temperature variability is strongly controlled by the onset of the monsoon and the marked seasonality typical of the region [*Kattel et al*., 2012]. The premonsoon and monsoon seasons are the warmest [*Shiraiwa et al*., 1992], and the diurnal temperature cycle is also strongly affected by this seasonality. During the monsoon, temperature fluctuations during the day are smaller [*Takahashi et al*., 1987; *Shiraiwa et al*., 1992; *Fujita et al*., 1998; *Fujita and Sakai*, 2000] as the thick cloud cover attenuates dissipation of heat through nocturnal surface radiative cooling [*Shiraiwa et al*., 1992].

While temporal variability is relatively well understood at both seasonal and diurnal scales, spatial variation is more complex, due to the steep and rough topography, development of valley and katabatic winds, and the presence of debris on many of the glacier tongues [*Fujita and Sakai*, 2000]. They concluded that constant lapse rates (LRs) should therefore not be used for melt calculations.

Little is known about variability of air temperature in the valley and how strong its elevation dependency is. Most of the previous studies in Langtang derived LRs from only a few points and did not analyze the strength of that relationship in terms of correlation [*Fujita and Sakai*, 2000]. *Kattel et al*. [2012] analyzed temperature LRs for the entire southern slopes of the central Himalayas in Nepal, and they found strong variability in the annual cycle of LRs, with the highest values in the premonsoon season, and minima in monsoon and winter. While the study of *Kattel et al*. [2012] has shed light on LRs variability, it focuses on a very large region and coarse temporal resolution, and LR variability at the catchment scale, where local processes may be important, remains largely unknown.

In this study we analyze seasonal observed LRs and precipitation gradients (PGs) based on a 2012–2013 field campaign in the Langtang valley in the greater Himalaya in Nepal (Figure 1). Our aim is to further our understanding of temperature and precipitation variability, to discuss their potential controlling mechanisms, and to test how sensitive simulations with a glaciohydrological model are to observed LRs and PGs.

1.1. Study Area

In this study we focus on the upper Langtang catchment in the central Himalaya in Nepal (Figure 1). The Langtang River is part of the Trishuli River system in the monsoon-dominated central part of the Himalayas. Its drainage area upstream of Syafru Besi is 585 km^2, of which 155 km^2 is glacierized. The glacier tongues below 5200 m are generally debris covered. The elevation ranges from 1406 m in Syafru Besi to the summit of Langtang Lirung at 7234 m. The Langtang River flows through the main valley (Figure 1), which is typically U shaped. The climate is dominated by monsoon circulation, with predominant easterly winds in the summer and westerly winds from October to May.

2. Data and Methods

2.1. Meteorological Setup

Following the main Langtang valley six tipping buckets and six temperature loggers were installed between Syafru Besi (1406 m above sea level (asl)) and Numthang (3981 m asl) (see Figure 1 and Table 1). At each site an ARG100 tipping bucket was mounted on a steel pole at about 1 m above the surface (Figure 2b). This low-cost tipping bucket is originally designed by the Institute of Hydrology, Wallingford, UK. The ARG100 has a funnel diameter of 254 mm, a funnel rim height of 340 mm, and a sensitivity of 0.2 mm of

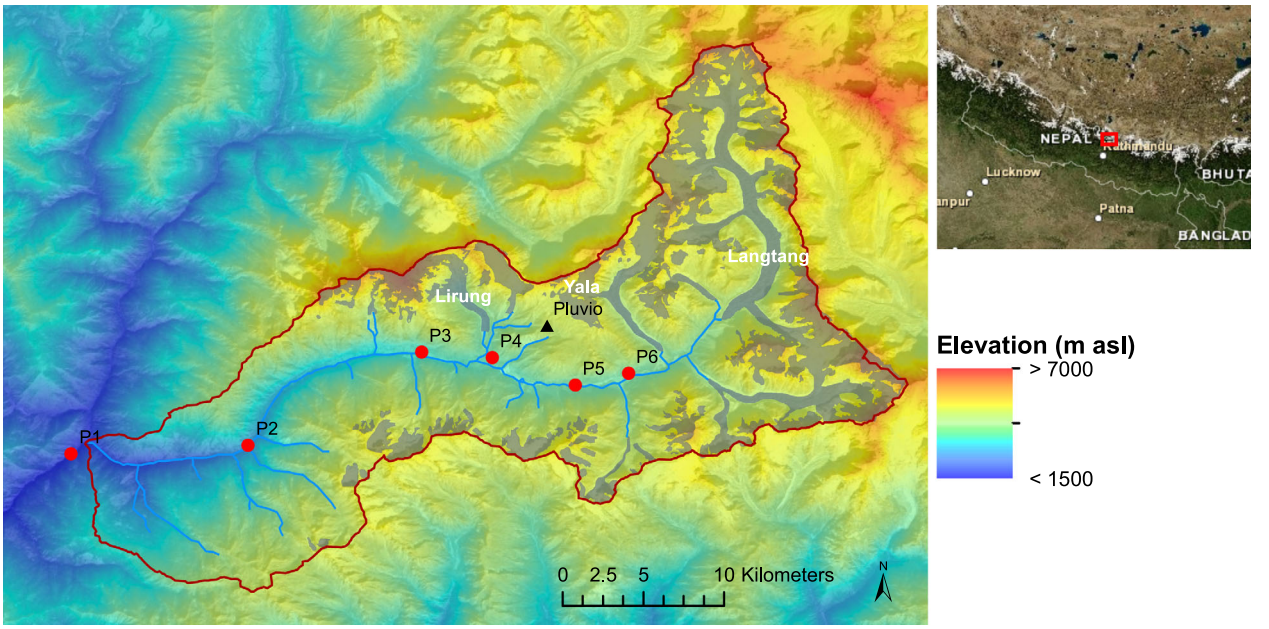

Figure 1. The Langtang River basin with outlet near Syafru Besi (P1), the location of the tipping buckets (P1–P6, red dots), and the high-altitude pluviometer (Pluvio, black triangle). The glaciers are shown in grey, and the names of several reference glaciers in white. Kyangjin is located at P4.

rain per tip. The ARG100 is equipped with a simple HOBO event data logger controlled using the dedicated BoxCar pro software. The temperature loggers (henceforth referred to as "TLoggers") are HOBO TidbiT v2 UTBI-001 from Onset. They were programmed to record air temperature at a 5 and 10 min interval. The loggers were fixed in PVC cylinders allowing natural ventilation through channelization of air flow and covered with an aluminum foil to shield the sensors from direct incoming shortwave radiation. Temperature measurements over snow surfaces are known to be strongly affected by radiation effects [*Huwald et al*., 2009], but given that all T-loggers are below the snow line the effect in this study will be limited. The cylinders were mounted on a metal pole at a distance of 2 m above the surface (see Figure 2c). They have an accuracy of 0.2°C in the range 0–50°C. Data were downloaded in August and October 2012 and in May 2013.

At an altitude of 4831 m asl on the slopes close to Yala glacier a more advanced pluviometer was installed that consists of an OTT Pluvio2 sensor, a Campbell SR50A sonic ranging sensor, and a Campbell temperature probe (109-L) (Figure 1 and Table 1). Hereafter the entire system consisting of the three sensors is referred to as Pluvio, whereas we refer to the precipitation gauge itself as Pluvio2. The Pluvio2 is based on the weighing principle, and it has an accuracy of 1% of the measured amount. The Pluvio2 has a capacity of 750 mm and measures both liquid and solid precipitations, and it complies with WMO (World Meteorological Organization, Geneva) guidelines for precipitation monitoring. The SR50A is a rugged, acoustic sensor that provides a noncontact method for determining snow depth. The SR50A determines depth by emitting an ultrasonic pulse and then measuring the elapsed time between the emission and return of the pulse. The 109-L sensor is a rugged, accurate probe that measures temperature of air, soil, or water from −50 to +70°C. It was placed in an unaspirated radiation shield (Campbell MET20) to avoid errors due to direct

Table 1. Overview of Stations, Locations, Elevation, and Sensors[a]

Description	Code	Latitude	Longitude	Average T (°C)	Elevation (m asl)	Relative Distance (m)	Sensors
Syafru Besi	P1	28.1574	85.3322	16.9	1406	0	TB, TL
Lama Hotel	P2	28.1621	85.4307	10.7	2370	9098	TB, TL
Langtang	P3	28.2140	85.5275	5.6	3539	18,563	TB, TL
Kyangjin	P4	28.2110	85.5669	4.0	3857	22,143	TB, TL
Jathang	P5	28.1956	85.6130	2.8	3875	26,206	TB, TL
Numthang	P6	28.2022	85.6428	2.8	3981	29,013	TB, TL
Near Yala	Pluvio	28.2290	85.5970	−1.8	4831	25,112	PL, UDG, TS

[a]TB, ARG100 tipping bucket; TL, Onset HOBO TidbiT v2 temperature logger; PL, OTT Pluvio2; UDG, Campbell SR50A sonic ranging sensor; TS, Campbell temperature probe 109-L inside radiation shield.

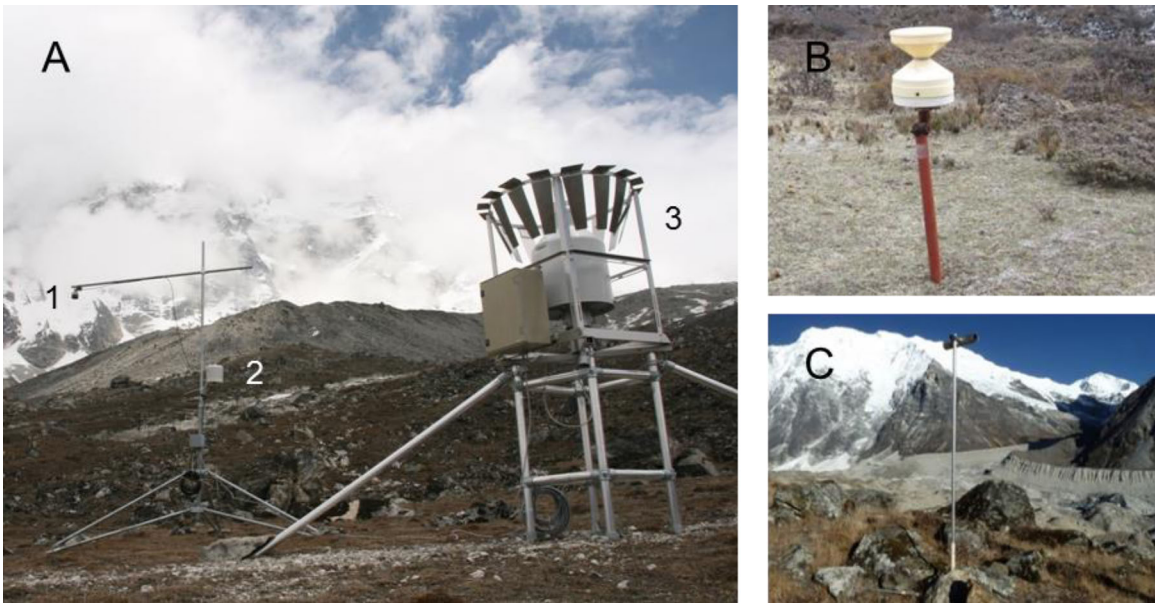

Figure 2. Setup of the instruments. (a) The high-altitude pluviometer (1, Campbell SR50A sonic ranging sensor; 2, Campbell temperature probe 109-L inside radiation shield; 3, OTT Pluvio2 including windshield), (b) a ARG100 tipping bucket, and (c) the Onset HOBO TidbiT v2 temperature logger inside its radiation shield.

radiation. The SR50A and the 109-L were installed on a tripod at 3 and 1.5 m heights above the surface, respectively. The Pluvio2 was installed on an aluminum scaffold, and the top of the Pluvio2 is at 2.5 m above the surface. The Pluvio2 includes a windscreen, and all sensors were connected to a Campbell CR200 data logger. Data of all three sensors were acquired at a 15 min interval. Data were downloaded, and batteries and antifreeze were replaced in October 2012 and May 2013.

2.2. Quality Control and Preprocessing

The data of the ARG100 tipping buckets, the temperature logger data, and the Pluvio data were all quality checked and the following corrections were made.

A yak was tied to the pole of the ARG100 at P5 sometime between 28 July and 8 August. This tilted the ARG100, and no precipitation was measured while there was considerable rainfall at P6. The P5 time series was corrected using the P6 precipitation and the average P5/P6 ratio on days with precipitation from the preceding period.

From 30 March 2013 onward the ARG100 at P2 was blocked by leaves, and no rainfall was observed from this date onward. The P2 time series was corrected using P3 precipitation and the average P2/P3 ratio on days with precipitation from the preceding period.

During the monsoon all tipping buckets were well below the snow line, but in some occasions during winter the temperature was below zero on days with precipitation. In those cases, the tipping bucket data were corrected using the Pluvio2 data and the ratio of the Pluvio2 data and the respective tipping bucket on days with above zero temperature.

Due to memory limitations and a delayed download, the TLogger's data record has a gap from 28 September until 1 November 2012. This period is not considered in the analysis. The TLogger in Kyangjin was not operating before 1 November; therefore, the data were replaced by temperature measurements from an automatic weather station at the same location.

The SR50-A data were corrected for the varying speed of sound as a result of air temperature variation.

2.3. Data Analysis

All tipping bucket data were aggregated to daily values, and the Pluvio data to both hourly and daily. Precipitation gradients were analyzed as a function of elevation, distance along the valley, latitude, and longitude both annually and seasonally. For the runs with the TOPKAPI-ETH model PGs were calculated from P4

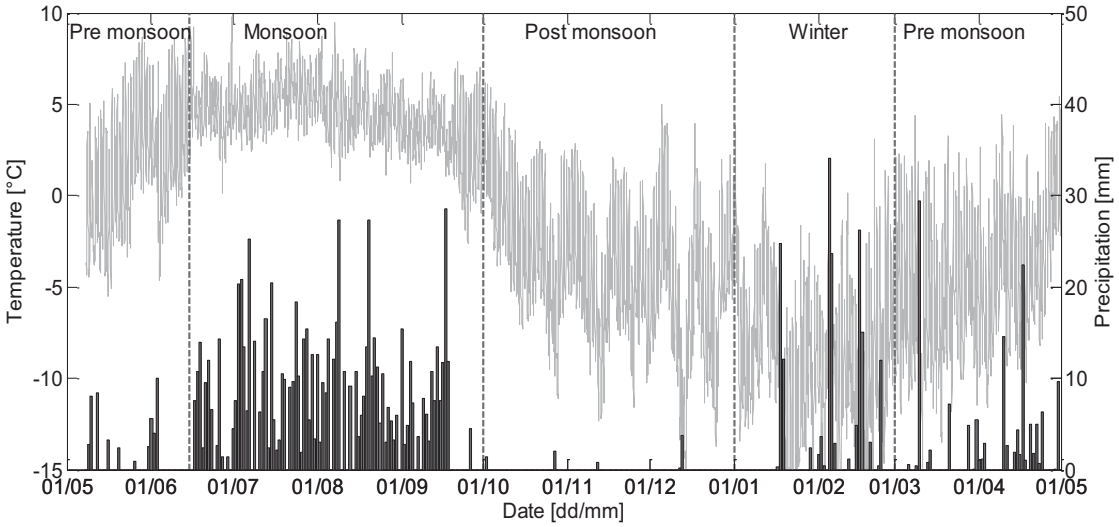

Figure 3. Daily precipitation (bars) and hourly temperature (grey line) at the location of the high-altitude pluviometer (Pluvio in Figure 1). The dotted vertical lines show the delineation of the different seasons.

upward. Both seasonal and annual PGs were derived, and distinction was made between a longitudinal and a vertical PG. These were derived by analyzing annual and seasonal precipitation sums of P4, P6, and Pluvio and their respective east-west distances and elevation differences, e.g., two linear equations with two unknowns were solved to derive the PGs. We define a vertical PG (% m^{-1}) as

$$PG = 100 \times \frac{P1 - P2}{z1 - z2} = \frac{dP}{dz} \quad (1)$$

where $P1$ and $P2$ are the precipitation sums of the highest and lowest points (in mm) and $z1$ and $z2$ are their respective elevations. For the longitudinal PG we use the same equation, but $z1 - z2$ is the distance between the two points. The longitudinal PG is positive from east to west by convention.

All temperature data were aggregated to hourly values for the analysis. Temperature lapse rates were calculated as a regression through all points in the temperature-elevation space [*Petersen and Pellicciotti*, 2011] and are a measure of how strongly temperature is linearly controlled by altitude. Air temperature is normally assumed to increase or decrease linearly with elevation [*Marshall and Sharp*, 2009] under well-mixed atmospheric conditions [*Lundquist et al.*, 2008], so that a LR (°C m^{-1}) can be defined as [*Petersen and Pellicciotti*, 2011]:

$$LR = \frac{T1 - T2}{z1 - z2} = \frac{dT}{dz} \quad (2)$$

where $T1$ and $T2$ are the air temperatures of the highest and lowest points (in °C), and $z1$ and $z2$ are their elevations (m). We calculate the LRs from regression of all values, as this allows calculating the strength of the relationship between air temperature and elevation [*Petersen and Pellicciotti*, 2011; *Kattel et al.*, 2012]. The measure of the strength of the altitudinal dependence is provided through the correlation coefficients of the linear regression. A strongly negative (steep) lapse rate indicates that temperature decreases rapidly with elevation, whereas the decrease is slower for a less negative (shallow) lapse rate [*Pepin and Losleben*, 2002; *Chutko and Lamoureux*, 2009; *Petersen and Pellicciotti*, 2011].

Temperature lapse rates were calculated for the entire year of record and separately for the main seasons. The seasons were identified based on the literature and from analysis of the precipitation and temperature records. Figure 3 shows the time series of air temperature and precipitation at the location of the Pluvio.

Based on these observations we define four distinct seasons.

Table 2. Overview of the Four Identified Seasons, Mean Temperature (T in °C), and Seasonal Precipitation (P in mm)

			P1		P2		P3		P4		P5		P6		Pluvio	
Season	Start	End	*T*	*P*	*T*	*P*	*T*	*P*	*T*	*P*	*T*	*P*	*T*	*P*	*T*	*P*
Premonsoon	8/5/12 1/3/13	14/6/12 30/4/13	23.6	107	15.8	98	10.1	156	7.8	142	7.5	156	7.6	136	1.9	181
Monsoon	15/6/12	30/9/12	20.7	960	14.9	1613	11.1	712	9.4	589	9.2	621	9.1	597	4.6	809
Postmonsoon	1/10/12	30/11/12	11.7	13	6.7	7	1.7	9	0.9	6	−1.9	7	−1.4	7	−3.8	8
Winter	1/12/11	28/2/13	15.2	135	8.2	102	2.0	98.8	0.2	130	−1.0	125	−1.2	132	−6.8	169

The premonsoon season from March to mid-June is characterized by relatively high temperatures gradually increasing toward the monsoon onset. The diurnal variability of temperature is high, and there are only few, rather small precipitation events.

The monsoon season lasts from mid-June until end of September. There is almost constant daily precipitation, and temperature is relatively high with small diurnal variability.

The postmonsoon season spans over the months of October, November, and December and shows nearly no precipitation and a steady decrease in temperature. Diurnal fluctuations of temperature increase again after the monsoon and are comparable to those of the premonsoon period.

The winter season (January and February) is characterized by the lowest temperatures, and precipitation occurs mostly in the form of snow at higher altitudes, with a few extreme events where daily precipitation exceeds the maximal values of monsoon precipitation.

This division agrees with what was reported by *Shiraiwa et al*. [1992] and *Kattel et al*. [2012]. The seasons, together with their mean temperature and precipitation, are summarized in Table 2. All results are reported separately for the four seasons defined above.

2.4. Glaciohydrological Modeling

We test the effect of using different precipitation gradients and temperature lapse rates on the outputs of a distributed glaciohydrological model. The model used for this purpose is the TOPKAPI-ETH model, which has been frequently used for simulations of glacier melt and runoff in high-elevation catchments [*Finger et al*., 2011, 2012; *Ragettli and Pellicciotti*, 2012; *Ragettli et al*., 2013a, 2013b]. The physical basis of the process representation allows setting up the model using data obtained locally, in ad hoc short-term field campaigns, to estimate model parameters [*Ragettli and Pellicciotti*, 2012].

The model requires daily input of measured precipitation and temperature, and station data from Kyangjin are used for this purpose. Daily cloud transmissivity coefficients are derived from the range of observed diurnal variations of air temperature at Kyangjin [*Pellicciotti et al*., 2011]. Temperature and precipitation are extrapolated to every model grid cell (resolution: 100 m) using spatially constant LRs and PGs.

Gravitational snow transport is simulated using a slope-dependent maximum snow holding depth [*Bernhardt and Schulz*, 2010]. If the snow depth of a model grid cell exceeds the cells' maximum snow holding depth, snow is redistributed to the next lower cell in flow direction. Snow and glacier melt in TOPKAPI-ETH are computed using an Enhanced Temperature-Index approach [*Pellicciotti et al*., 2005, 2008]. The model was thoroughly set up and tested using an extensive data set collected in 2012–2013, and calibration was conducted against data of different nature [*Ragettli and Pellicciotti*, 2013]. Melt parameters are estimated using data from ablation stake measurements on Lirung and Yala glacier (Figure 1) during the period November 2011 to May 2013 [*Ragettli and Pellicciotti*, 2013]. Melt parameters are different for debris-covered and debris-free glacier areas, in order to take into account the melt reducing effect of the thick debris cover observed on many glaciers within the study area. Validation of the simulated snow cover recession after winter (March–June) against Moderate Resolution Imaging Spectroradiometer (MODIS)/Terra and MODIS/Aqua daily fractional snow cover indicates very good model performance. The coefficient of determination (r^2) for the period 2012–2013 between daily observed and daily simulated snow cover was 0.92 using Aqua satellite data and 0.93 using Terra satellite data.

In this study, we run the model with five different combinations of the observed LRs and PGs, and we compare the results with a reference run where precipitation is constant with increasing elevation and the

Table 3. Configuration of TOPKAPI-ETH Model Runs[a]

	PGv	PGh	LR
Reference run			ELR
Run 1			Mean annual observed
Run 2			Mean seasonal observed
Run 3	Mean annual observed	Mean annual observed	ELR
Run 4	Mean seasonal observed	Mean seasonal observed	ELR
Run 5	Mean seasonal observed	Mean seasonal observed	Mean seasonal observed

[a]PGv and PGh are the vertical and horizontal precipitation gradients, and LR is the temperature lapse rate. The values of PGv and PGh can be found in Table 4.

Table 4. Vertical (PGv) and Longitudinal (PGh) Precipitation Gradients in % m^{-1}

Season	PGv	PGh
Premonsoon	0.031	−0.0004
Monsoon	0.040	−0.0005
Postmonsoon	0.039	0.0022
Winter	0.053	0.0006
Annual	0.041	−0.0003

standard environmental lapse rate (ELR, −0.0065°C/m) is used to extrapolate temperature data. The configurations of the different runs are reported in Table 3. The values of observed seasonal and annual LRs are shown in Table 5. For assessing how sensitive a glaciohydrological model is to PGs we consider only the area from P4 upward, as the TOPKAPI-ETH model is available from the stream gauge at P4 upward, and there is a more consistent longitudinal and vertical PG from P4 upward. The PGs used to force the model are shown in Table 4. The model is forced with precipitation and temperature data from the Department of Hydrology and Meteorology for a period of 8 years (2003–2010). The first year is used to initialize the simulations. We therefore discuss mean differences in model outputs with respect to the reference run for the period 2004–2010.

3. Results and Discussion

3.1. Precipitation

Figure 4 shows the seasonal precipitation sums and wet day frequencies. There is a strong variation in precipitation in the valley over short horizontal distances. The maximum precipitation is at P2 (1819 mm), and the minimum precipitation is at P4 (867 mm), e.g., a 52% decrease of precipitation within a distance of 14 km. P2 is the wettest location only during the monsoon, and since P2 is located after the first steep ascend in the valley (Table 1), it seems plausible that the wet convective monsoon air mass is orographically forced at this elevation. During winter and the premonsoon this is not observed, and this may be related to differences in circulation patterns and a more stratiform type of precipitation. The majority of rainfall falls during the monsoon, and this ranges from 68% of the annual precipitation in P4 to 89% in P2. There is also strong variation in the wet day frequencies (Figure 4). During the monsoon there is precipitation nearly every day ranging from 70% of the days at Pluvio to 86% at P5. In winter the wet day frequencies are much lower, and there is only occasional precipitation ranging from 17% (P1) to 31% (P6) of the total number of days.

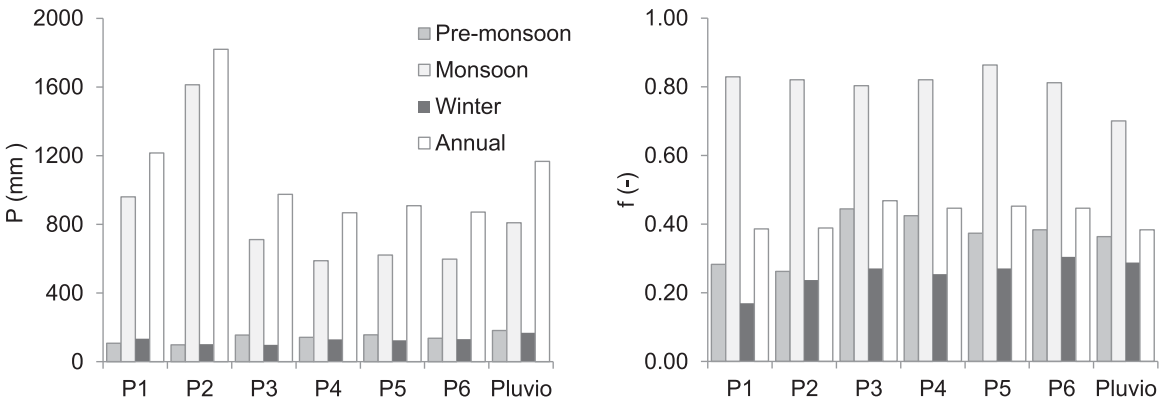

Figure 4. Annual, premonsoon, monsoon, and winter (left) precipitation sums and (right) wet day frequency based on observations from 8 May 2012 until 30 April 2013.

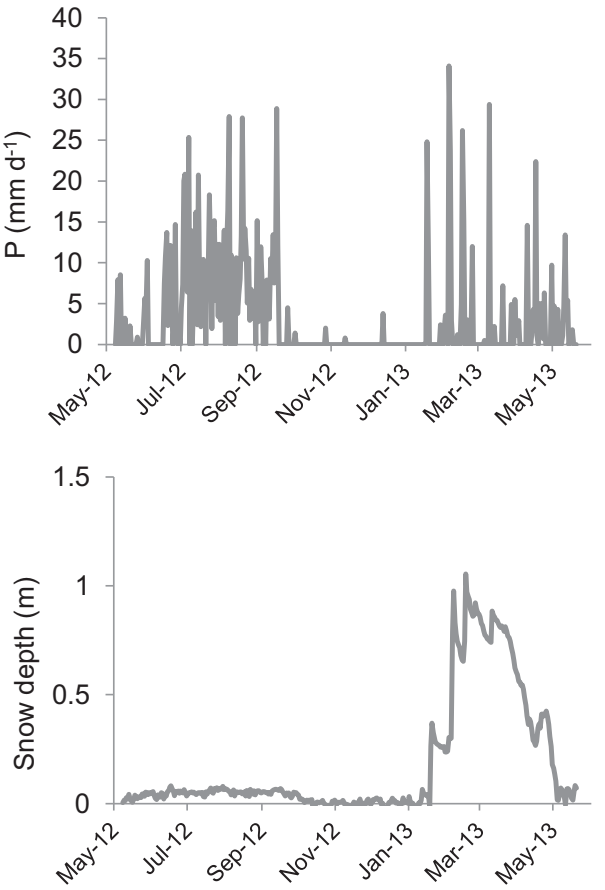

Figure 5. (top) Daily precipitation and (bottom) snow depth at Pluvio.

There are also considerable differences in the daily precipitation intensities during both the monsoon and winter seasons. The most extreme precipitation occurred in P2 during the monsoon (58 mm/d). No clear spatial trends can be identified in the rainfall intensities. Although the wet day frequency is much lower during the winter, the precipitation intensities are generally higher. The distribution of the intensities during winter is more skewed than the monsoon intensities, e.g., during winter there are a few events with a relatively extreme amount of precipitation, whereas during the monsoon the intensities are more or less normally distributed around the mean.

The premonsoon shows a clear diurnal precipitation pattern. During the morning it is relatively dry and most precipitation occurs during the later afternoon (5.00–7.00 P.M.), decreasing again during the evening and the night. During the other seasons we also observe a diurnal pattern, but without the distinct peak during the late afternoon. This distinct peak may be explained by the fact that the air is already relatively moist in this season, which in combination with relatively abrupt radiative cooling results in the late afternoon peak during the premonsoon.

We analyzed large-scale wind direction and speed using *u* and *v* winds at the geopotential height of 500mb derived from the ERA-INTERIM reanalysis data set [*Dee et al.*, 2011]. The analysis shows a distinct intraannual pattern. During winter, 500 mb wind speeds are much higher than during monsoon. In winter, there is a strong northwestern wind from the Tibetan plateau, whereas during the monsoon the wind comes from the southeast. This is in agreement with the mechanisms which we outline in section 1.

No consistent trend in the entire valley is evident between precipitation and elevation, relative distance along the valley, longitude, or latitude. We hypothesize that during monsoon there is a strong upvalley wind that leads to the formation of convective cumulus clouds during the day, and this causes a strong precipitation peak at P2 after the first steep ascent in the valley. Even at night weak upvalley winds continue to flow during the monsoon, because radiative cooling is suppressed due to the presence of stratus in the evening [*Seko*, 1987]. In winter, precipitation is associated with synoptic scale disturbances of stratiform type, with less pronounced diurnal variation and a stronger elevation dependence [*Seko*, 1987].

From P4 upward, PGs can be discerned, and the PGs that were used in the glaciohydrological modeling are shown in Table 4. A positive vertical PG is observed in all seasons that ranges from 31% to 53% increase in precipitation over a 1000 m in elevation rise during the premonsoon and winter, respectively. Calculated longitudinal PGs are negative during premonsoon and monsoon and positive during winter, and several studies have used or suggested the existence of longitudinal gradients [*Seko*, 1987; *Konz et al.*, 2007; *Immerzeel et al.*, 2012b].

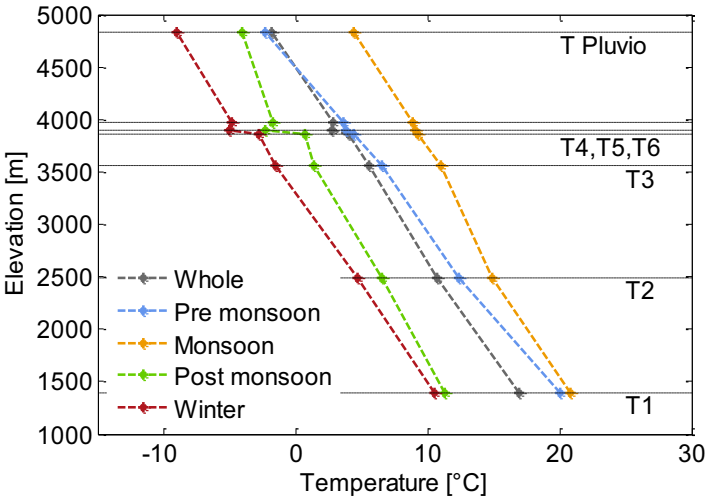

Figure 6. Mean temperature at all locations plotted against elevation for the entire period (8 May 2012 to 1 May 2013), premonsoon, monsoon, postmonsoon, and winter.

During winter a significant part of the precipitation falls in the form of snow at high altitude (Figure 5). The first snow fall occurred on 18 January 2013, and the maximum snow depth at Pluvio was 1.1 m on 17 February 2013. By 4 May 2013 the snowpack was completely depleted. Snow falls during a few isolated events only, and there were only 6 days when there was more than 10 cm of increase in snow depth. By using the total precipitation and snow depth increments on these days we estimate that the average density of the fresh snow falling on those days is 115 $\pm$ 48 kg m^{-3}. In total we estimate that 211 mm falls in the form of snow (17.5% of the annual precipitation).

3.2. Temperature

The mean temperatures versus elevation at all locations are shown in Figure 6, and the corresponding LRs calculated from linear regression are reported in Table 5. The increase in temperature from winter to monsoon is obvious throughout the valley. Temperature and elevation are highly correlated (Table 5), indicating that the relationship is strong, and temperature can be predicted accurately as a function of elevation [*Kattel et al.*, 2012].

Figure 6 also shows that the linearity in the elevation-temperature relation seems to be interrupted during winter and postmonsoon for P4 and P5. These are the coldest seasons and the atmosphere is stable. In combination with the fact that beyond P4 the valley widens and the slopes become less steep, cold air pooling may explain this anomaly in LR [*Lundquist et al.*, 2008].

While temperatures are highest during monsoon, the LR (−0.0046°C/m) is less negative than in winter (−0.0058°C/m) as during monsoon the temperature decrease with elevation is attenuated by the presence of a consistent cloud cover, which reduces radiative cooling. Premonsoon season has the steepest lapse rate (−0.0064°C), indicating that differences in temperature between the locations are largest during this time, whereas the postmonsoon season shows a LR (−0.0049°C/m) similar, but slightly steeper, than during monsoon. The most prominent reasons for the seasonal differences in LRs are differences in relative humidity. Under humid conditions, such as during the monsoon, the condensation of water droplets warm the air during lifting, resulting in more shallow LRs.

The peak in LR in premonsoon season is consistent with the observations for the entire southern slopes of the central Himalayas and might also be related to the vertical gradient of premonsoon snow cover, e.g., deep snow cover at high elevations and none at lower elevations [*Kattel et al.*, 2012]. Snow-covered surface has a high albedo and from the limited net radiation that remains a significant part, is used for snow melt. The sensible heat flux is therefore generally limited, which in combination with strong radiative cooling from the cold surface, results in relatively low air temperatures. In addition, some of the differences among

Table 5. Mean, Minimum, and Maximum Values of the Diurnal Cycle for Lapse Rate (LR) and Correlation (*r*) for the Seasons of Premonsoon, Monsoon, Postmonsoon, and Winter Between Mean, Minimum and Maximum Temperatures

Season	Mean LR (°C/m)	Minimum LR (°C/m)	Maximum LR (°C/m)	Mean *r*	Minimum *r*	Maximum *r*
Premonsoon	−0.0064	−0.0070	−0.0054	0.989	0.943	0.997
Monsoon	−0.0046	−0.0053	−0.0040	0.990	0.956	0.997
Postmonsoon	−0.0049	−0.0059	−0.0034	0.944	0.814	0.982
Winter	−0.0058	−0.0067	−0.0045	0.969	0.900	0.987

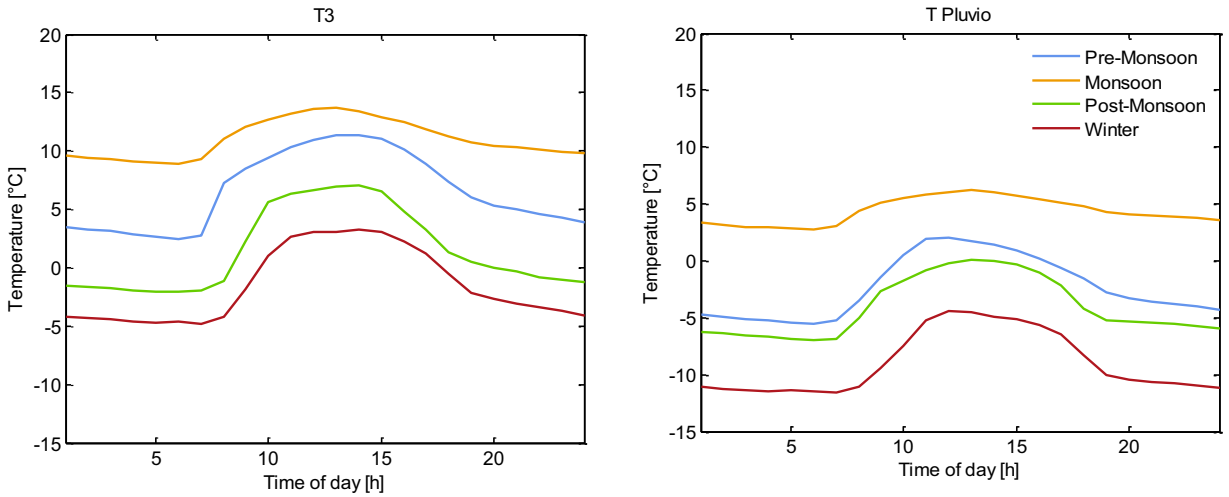

Figure 7. Mean diurnal cycle temperature at P3 and Pluvio for the premonsoon season (blue), monsoon season (orange), postmonsoon season (green), and winter season (red line).

locations during premonsoon might be explained to changing weather patterns within the valley (scattered showers, partial cloud cover, and partial clear sky with high incoming radiation), whereas in postmonsoon the climate is stable with high incoming shortwave radiation flux.

Over all seasons, and especially during monsoon and postmonsoon, the observed LRs are shallower than the values of the commonly used ELR of −0.0065°C/m, indicating that in the Langtang valley, the decrease of air temperature with elevation is less rapid than commonly assumed for free atmosphere conditions. This is important for redistribution of air temperature used to force glaciohydrological models, as use of the ELR would result in lower air temperatures in the upper sections of the valley and higher temperatures in the lower sections. The mean annual observed lapse rate (−0.0054°C/m), which is also lower than the ELR, is an average of distinct seasonal values that we consider separately for glaciohydrological modeling (Table 3).

Our results generally agree with studies in other mountainous regions of the world [*Minder et al*., 2010; *Mizukami et al*., 2013]. *Minder et al*. [2010], for example, find for the Cascade mountain range in the United States LR ranging between −0.0039 and −0.0052°C/m with strong seasonal variation and the most shallow LRs during the season with the highest relative humidity. They also show that a high-resolution mesoscale weather model (MM5) is capable of accurately simulating the observed LRs, probably due to accurate simulation of spatiotemporal variations in atmospheric moisture. Although such models are currently unavailable for the Himalaya, it would certainly be recommendable for a future study to explain the physical processes underlying Himalayan LR variation.

Figure 7 shows that the diurnal range is strongly reduced during the monsoon, and this can be attributed to the influence of a thick cloud cover [*Takahashi et al*., 1987; *Shiraiwa et al*., 1992]. The diurnal range generally decreases with altitude.

The regression lapse rate through all locations for every hour of the day was calculated for all four seasons, and values are reported in Table 5 together with the corresponding correlation coefficients. Correlation coefficients for *mean* and *maximum* temperature LRs are very high, especially for the maximum temperature LRs, and vary between 0.944 and 0.997 (Table 5). However, correlation coefficients between *minimum* temperature and elevation are lower and more variable, with values between 0.814 and 0.956 (Table 5). This indicates that the relationship between temperature and elevation for low temperature is weaker and other factors have an influence [*Kattel et al*., 2012]. Several studies have suggested that factors such as humidity, cloudiness, wind velocity, valley orientation, and the general drainage patterns of cold air from higher grounds are stronger controls over minimum temperature than elevation [*Lundquist et al*., 2008; *Gouvas et al*., 2011]. The very high correlation for *maximum* temperature-elevation relationship seems on the opposite to indicate that elevation is the main control on air temperature variability under high temperature conditions, which occur mainly during the day (Figure 7). Correlation coefficients between *mean* temperature

Table 6. Median and Standard Deviation (σ) of the Simulated Equilibrium Line Altitude (ELA) at Yala Glacier (5130–5750 m asl) of Each Run

	Median (m asl)	σ (m)
Reference run	ELA below glacier	
Run 1	5264	33
Run 2	5510	54
Run 3	ELA below glacier	
Run 4	ELA below glacier	
Run 5	5403	26

and elevation are lowest in postmonsoon and winter, increase in March–May, and reach the highest values during monsoon (with a value of 0.990), in very good agreement with findings from *Kattel et al.* [2012]. The lower correlation coefficients during postmonsoon and winter have also been attributed to inversions [*Kattel et al.*, 2012].

The LRs found here result in temperature differences up to several degrees over the elevation range typical of the Langtang catchment, and their diurnal variability temperature is relevant for numerous processes, such as melt and evapotranspiration, all occurring within certain periods of the day.

3.3. Glaciohydrological Model Simulations

We test the effect of the observed PGs and LRs on the sensitivity of the outputs of the TOPKAPI-ETH glaciohydrological model using the five runs listed in Table 3. Runs 1 and 2 are to examine impact of different LRs (observed annual LR versus seasonal LR), runs 3 and 4 are for assessing the impact of different PGs (annual mean versus seasonal PG), and run 5 is used to show impact of combination of seasonal PGs and LRs. Run 5 can be considered as the optimum run using the best information available. The simulated equilibrium line altitude (ELA) values for Yala glacier—a benchmark glacier in the region—are consistent with information from the literature: field-based measurements locate the ELA at Yala at about 5400 m [*Sugiyama et al.*, 2013]. The median elevation of the simulated ELA by run 5 for the period 2004–2010 is exactly 5403 m asl (with a standard deviation of 26 m between different years, Table 6). The simulated ELA at Yala by the other

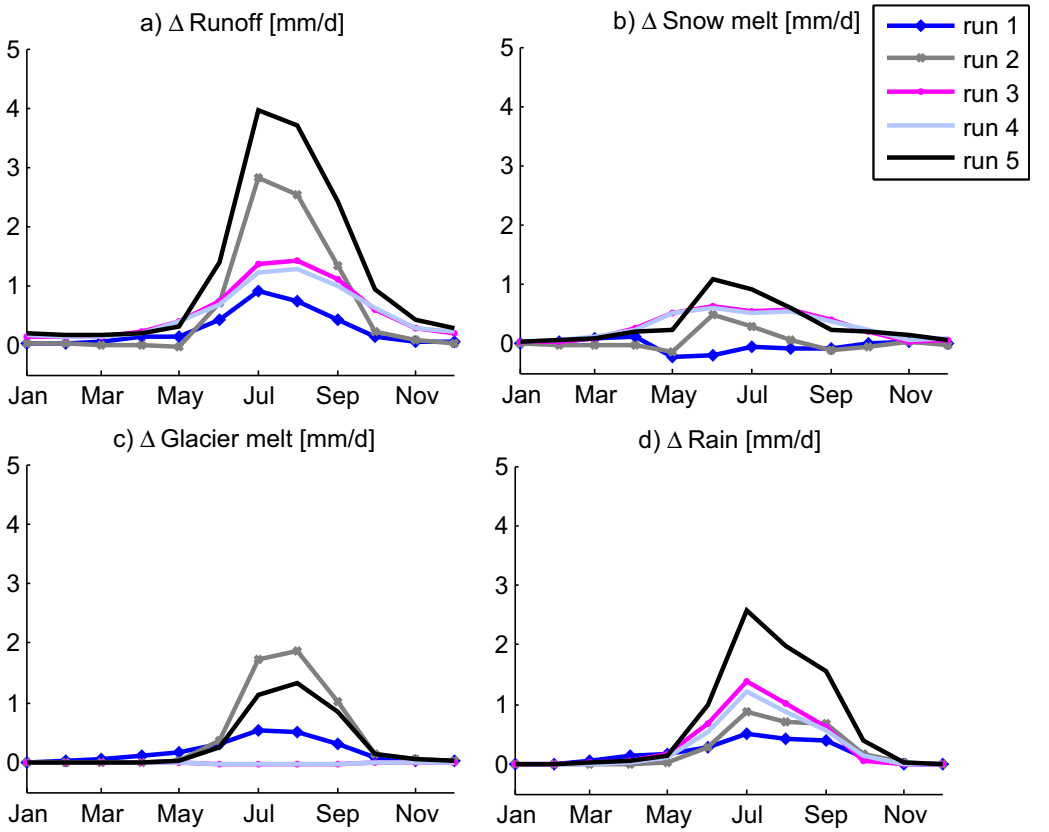

Figure 8. Effect of using different configurations for precipitation gradients and temperature lapse rates on mean monthly simulated runoff, snow melt, glacier melt, and rain. The figure shows the monthly mean differences with respect to the reference run (run-reference run) (Table 3), simulated for the period 2004–2010.

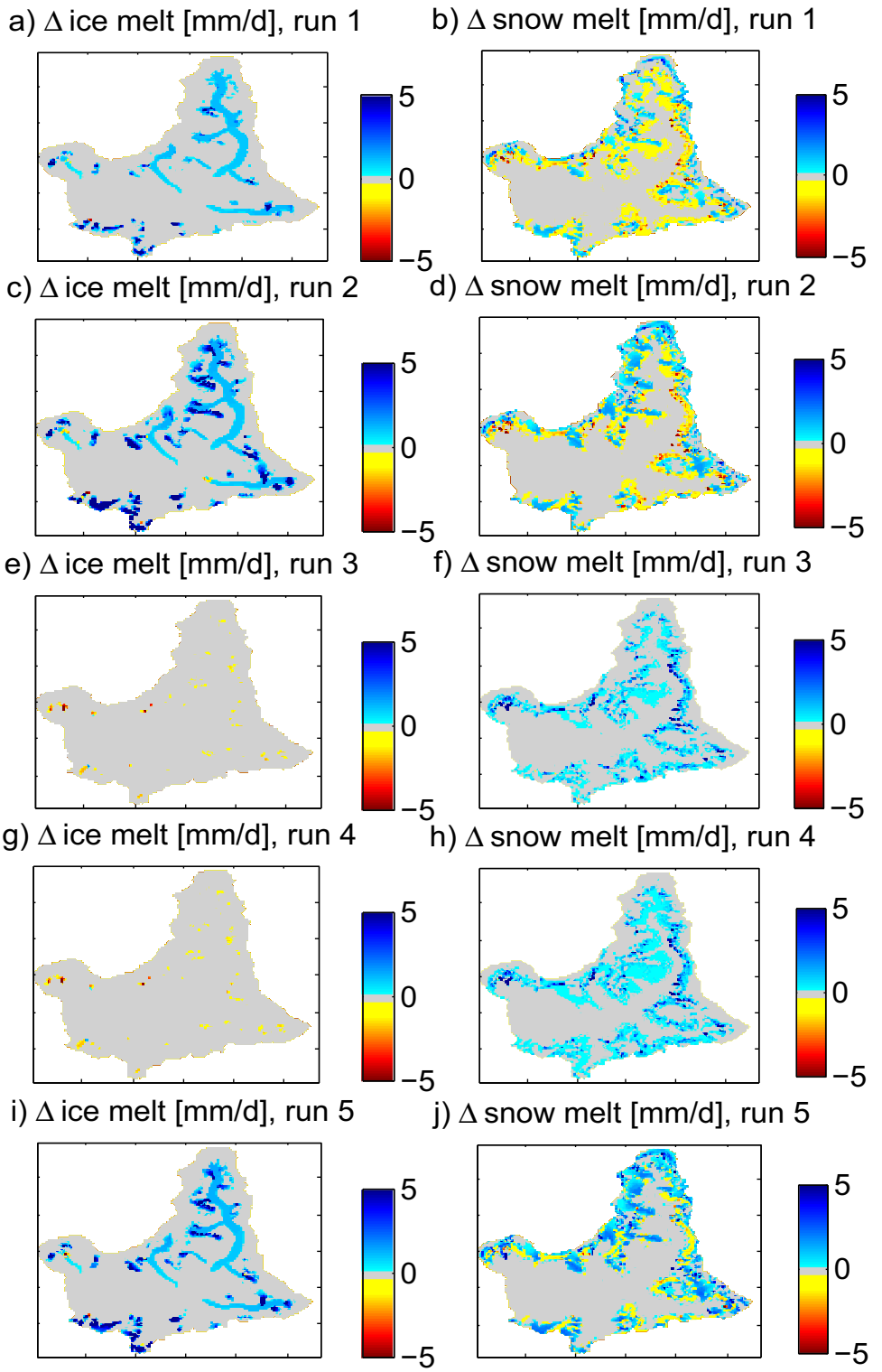

Figure 9. Effect of using different configurations for precipitation gradients and temperature lapse rates on the spatial distribution of mean annual simulated runoff, snow melt, glacier melt, and rain. The maps show the differences with respect to the reference run (run-reference run; Table 3) simulated for the period 2004–2010.

runs is mostly below that value (reference run, run 1, runs 3 and 4) or above (run 2). Validation against measured streamflow—the most common approach to validate glaciohydrological models—is not possible for Langtang because reliable streamflow data are not available for this period.

In runs 1 and 2 the temperatures are higher because the observed temperature lapse rates are shallower than the ELR. But since precipitation remains the same as for the reference run, less snow accumulation and more rain at lower elevations are simulated. Consequently, at lower elevations the model simulates also less snowmelt (yellow areas in Figures 9b and 9d). At higher elevations, in the accumulation areas of glaciers where annual snow accumulation exceeds annual snowmelt, the model simulates more snowmelt because of higher temperatures. Glacier-ice melt increases owing to less snow on glaciers and more melt due to higher temperatures (Figures 8c, 9a, and 9c). The highest increases of runoff, snow melt, and ice melt are simulated for run 2 and during July and August, due to very shallow temperature lapse rates during the monsoon period.

In runs 3 and 4 the overall precipitation is higher. With respect to the reference run, negative horizontal valley gradients lead only to less precipitation in a very small portion of the catchment, the valley bottom east of Kyangjin, where most of the precipitation falls in the form of rain. Everywhere else precipitation is higher due to the application of the observed steep elevation gradients. As the snow/rain transition remains at the same elevation as for the reference run, we simulate more snowfall and for areas below the equilibrium line altitude, more snowmelt (blue areas in Figures 9f and 9h). Overall simulated ice melt does not change significantly (Figure 8c). More snow accumulation also means more redistribution of snow due to gravitational snow transport. As a consequence, snowmelt below steep slopes increases disproportionately to the increases in precipitation (dark blue areas in Figures 9f and 9h). Since the thicker snowpack persists for a longer period on top of the glacier ice, increased avalanching can at some places significantly reduce ice melt (as it is the case for some Lirung glacier grid cells, dark red pixels in Figures 9e and 9g).

Concerning run 5, the mean monthly differences to the reference run are proportional to the differences reported for run 2, where the same temperature lapse rates were used (Figure 8a). Ice melt increases with respect to the reference run, despite more precipitation, but slightly less than in run 2 (Figure 8c). These model results suggest that the system is very sensitive to both changes in LRs and PGs: the effect of changing both at the same time leads to the strongest increase of simulated runoff with respect to the reference run (Figure 8a). However, using the observed monsoon temperature LRs for simulations (runs 2 and 5) has the most significant effect on simulated runoff, comparing to the other runs and the case where no observed data are used for simulations.

Based on these results, we therefore stress the importance of using observed LRs and PGs in glaciohydrological modeling studies, and also studies in other regions of the world confirm this [*Petersen and Pellicciotti*, 2011; *Pellicciotti et al*., 2014]. Short-term, low-cost campaigns can already provide crucial information that will greatly enhance the quality of such simulations.

4. Conclusions

In this study we analyze observed LRs and PGs acquired during a 1 year field campaign in 2012–2013 in the Langtang catchment in the central Himalaya in Nepal. We use these observations to improve our understanding of precipitation and temperature patterns in a catchment with extreme relief, and we discuss possible controlling mechanisms. We also illustrate how sensitive simulations with a glaciohydrological model are to observed LRs and PGs, and we draw the following conclusions.

There are four clearly detectable seasons over the year: a premonsoon season with a gradual increase in temperature and occasional precipitation; the monsoon season with daily precipitation, high temperatures, and a reduced diurnal range in temperature; a postmonsoon seasons with no precipitation and a gradual decrease in temperature; and the winter season with very low temperatures and frequent precipitation in the form of strong events and snowfall.

The precipitation patterns are complex, and PGs for the entire valley cannot be derived. There is a strong seasonal difference in the precipitation patterns and their controlling mechanisms. In the upper part of the catchment we do however identify a positive PG, which on an annual basis is 41% per 1000 m elevation rise. Our highest precipitation gauge was located at 4831 m, and despite the logistical constraints, it is important to extend the monitoring of precipitation at this and higher altitudes to be able to better constrain PGs and identify the altitude with maximum precipitation per season. The variation we identify also suggests that the use of satellite derived [*Huffman et al*., 2007] or large-scale gridded precipitation products

[*Yatagai et al*., 2012], which have a resolution in the order of 25 km, are questionable without further spatial downscaling using local information. The way precipitation fields are generated for glaciohydrological models needs to be reconsidered, and the use of field radars, hyperresolution weather models, and innovative proxies [*Immerzeel et al*., 2012a] is needed to further our understanding of precipitation dynamics in a monsoon-dominated climate with extreme topography.

The temperature analysis shows that valley LRs exist, and that there is a high correlation between temperature and elevation for all seasons. However, the LRs are shallower than the ELR, and there is high temporal variability on a seasonal and diurnal scale. These findings confirm other studies in mountain regions in the United States [*Minder et al*., 2010; *Mizukami et al*., 2013]. Both the temporal variability and the specific values should therefore be taken into account when generating input fields to glacier mass balance and runoff models.

LRs and PGs have a very large impact on the outputs of the glaciohydrological model used. The impact of the LRs is particularly large, and in specific months an increase of glacier melt of 400% is modeled. This is caused by the fact that the critical elevation below which snow falls as rain and below which melt occurs moves up just above the tongues of the main glaciers, and as a result the melt is amplified. Temperature measurements are relatively cheap, and a single year of observations has already great added value in constraining model parameters. Only the model run using measured seasonal LRs and PGs produces model output that compares well with observations of the ELA at Yala glacier, a benchmark glacier in the region [*Sugiyama et al*., 2013]. The Himalaya region is in urgent need for more complete analyses regarding the health of its glaciers [*Cogley*, 2011]. Our results are therefore of high relevance, given the fact that modeling studies are required to bridge the gap between process understanding at the point scale and remote sensing studies focusing on glacier changes.

Acknowledgments

The authors thank Mark Williams, Jessica Lundquist, and one anonymous reviewer for their constructive suggestions for improving this manuscript. The authors are grateful to all the people who assisted with the data collection, and in particular, Prashant Baral, Sonika Shahi, Martin Heynen, and Simon Wicki. The authors are very grateful to the HKH Cryosphere Monitoring Project implemented by the International Centre for Integrated Mountain Development (ICIMOD) and supported by the Norwegian Ministry of Foreign Affairs. They would also like the thank the project partners for their help in carrying out this study and for providing data in particular the Himalayan Cryosphere, Climate and Disaster Research Center of Kathmandu University and the Department of Hydrology and Meteorology and the Department of National Parks and Wildlife Conservation of the Government of Nepal. This study was partially funded by the Netherlands Organization for Scientific Research through their VENI program and by the South Asia Research Hub of the UK Department for International Development (DFID).

References

Bernhardt, M., and K. Schulz (2010), SnowSlide: A simple routine for calculating gravitational snow transport, *Geophys. Res. Lett.*, *37*, L11502, doi:10.1029/2010GL043086.

Bookhagen, B., and D. W. Burbank (2006), Topography, relief, and TRMM-derived rainfall variations along the Himalaya, *Geophys. Res. Lett.*, *33*, L08405, doi:10.1029/2006GL026037.

Chutko, K. J., and S. F. Lamoureux (2009), The influence of low-level thermal inversions on estimated melt-season characteristics in the central Canadian Arctic, *Int. J. Climatol.*, *29*(2), 259–268, doi:10.1002/joc.1722.

Cogley, J. G. (2011), Present and future states of Himalaya and Karakoram glaciers, *Ann. Glaciol.*, *52*(59), 69–73.

Dee, D. P., et al. (2011), The ERA-Interim reanalysis: Configuration and performance of the data assimilation system, *Q. J. R. Meteorol. Soc.*, *137*(656), 553–597, doi:10.1002/qj.828.

Finger, D., F. Pellicciotti, M. Konz, S. Rimkus, and P. Burlando (2011), The value of glacier mass balance, satellite snow cover images, and hourly discharge for improving the performance of a physically based distributed hydrological model, *Water Resour. Res.*, *47*, W07519, doi:10.1029/2010WR009824.

Finger, D., G. Heinrich, A. Gobiet, and A. Bauder (2012), Projections of future water resources and their uncertainty in a glacierized catchment in the Swiss Alps and the subsequent effects on hydropower production during the 21st century, *Water Resour. Res.*, *48*, W02521, doi:10.1029/2011WR010733.

Fujita, K., and A. Sakai (2000), Air temperature environment on the debris-covered area of Lirung Glacier, Langtang Valley, Nepal Himalayas, in *Debris-Covered Glaciers*, edited by M. Nakawo, C. F. Raymond, and A. Fountain, *IAHS Publ. 264*, pp. 83–88. Int. Assoc. of Hydrol. Sci., Wallingford, U. K.

Fujita, K., N. Takeuchi, and K. Seko (1998), Glaciological observations of Yala Glacier in Langtang Valley, Nepal Himalayas, 1994 and 1996, *Bull. Glacier Res.*, *16*, 75–81.

Gouvas, M. A., N. K. Sakellariou, and H. D. Kambezidis (2011), Estimation of the monthly and annual mean maximum and mean minimum air temperature values in Greece, *Meteorol. Atmos. Phys.*, *110*, 143–149, doi:10.1007/s00703-010-0111-y.

Huffman, G. J., R. F. Adler, D. T. Bolvin, G. Gu, E. J. Nelkin, K. P. Bowman, Y. Hong, E. F. Stocker, and D. B. Wolff (2007), The TRMM Multisatellite Precipitation Analysis (TMPA): Quasi-global, multiyear, combined-sensor precipitation estimates at fine scales, *J. Hydrometeorol.*, *8*(1), 38–55, doi:10.1175/JHM560.1.

Huwald, H., C. W. Higgins, M.-O. Boldi, E. Bou-Zeid, M. Lehning, and M. B. Parlange (2009), Albedo effect on radiative errors in air temperature measurements, *Water Resour. Res.*, *45*, W08431, doi:10.1029/2008WR007600.

Immerzeel, W. W., L. P. H. Van Beek, and M. F. P. Bierkens (2010), Climate change will affect the Asian water towers, *Science*, *328*(5984), 1382–1385, doi:10.1126/science.1183188.

Immerzeel, W. W., F. Pellicciotti, and A. B. Shrestha (2012a), Glaciers as a proxy to quantify the spatial distribution of precipitation in the Hunza basin, *Mt. Res. Dev.*, *32*(1), 30–38, doi:10.1659/MRD-JOURNAL-D-11–00097.1.

Immerzeel, W. W., L. P. H. Beek, M. Konz, a. B. Shrestha, and M. F. P. Bierkens (2012b), Hydrological response to climate change in a glacierized catchment in the Himalayas, *Clim. Change*, *110*, 721–736, doi:10.1007/s10584-011-0143-4.

Kattel, D. B., T. Yao, K. Yang, L. Tian, G. Yang, and D. Joswiak (2012), Temperature lapse rate in complex mountain terrain on the southern slope of the central Himalayas, *Theor. Appl. Climatol.*, *113*(3–4), 671–682, doi:10.1007/s00704-012-0816-6.

Konz, M., S. Uhlenbrook, L. Braun, A. Shrestha, and S. Demuth (2007), Implementation of a process-based catchment model in a poorly gauged, highly glacierized Himalayan headwater, *Hydrol. Earth Syst. Sci.*, *11*(1993), 1323–1339.

Lundquist, J. D., N. Pepin, and C. Rochford (2008), Automated algorithm for mapping regions of cold-air pooling in complex terrain, *J. Geophys. Res.*, *113*, D22107, doi:10.1029/2008JD009879.

Marshall, S. J., and M. J. Sharp (2009), Temperature and melt modeling on the Prince of Wales Ice Field, Canadian High Arctic, *J. Clim.*, *22*(6), 1454–1468, doi:10.1175/2008JCLI2560.1.
Minder, J. R., P. W. Mote, and J. D. Lundquist (2010), Surface temperature lapse rates over complex terrain: Lessons from the Cascade Mountains, *J. Geophys. Res.*, *115*, D14122, doi:10.1029/2009JD013493.
Mizukami, N., M. Clark, A. Slater, L. Brekke, M. Elsner, J. Arnold, and S. Gangopadhyay (2013), Hydrologic implications of different large-scale meteorological model forcing datasets in mountainous regions, *J. Hydrometeorol.*, doi:10.1175/JHM-D-13-036.1, in press.
Pellicciotti, F., B. Brock, U. Strasser, P. Burlando, M. Funk, and J. Corripio (2005), An enhanced temperature-index glacier melt model including the shortwave radiation balance: Development and testing for Haut Glacier d'Arolla, Switzerland, *J. Glaciol.*, *51*(175), 573–587.
Pellicciotti, F., J. Helbing, V. Favier, and J. Corripio (2008), A study of the energy balance and melt regime on Juncal Norte Glacier, semi-arid Andes of central Chile, using melt models of different complexity, *Hydrol. Processes*, *22*(19), 3980–3997, doi:10.1002/hyp.7085.
Pellicciotti, F., T. Raschle, T. Huerlimann, M. Carenzo, and P. Burlando (2011), Transmission of solar radiation through clouds on melting glaciers: A comparison of parameterisations and their impact on melt modelling, *J. Glaciol.*, *57*, 367–381.
Pellicciotti, F., M. Konz, W. W. Immerzeel, and A. B. Shrestha (2012), Challenges and uncertainties in hydrological modelling of remote Hindu Kush-Himalayan (HKH) basins: Suggestions for calibration strategies, *Mt. Res. Dev.*, *32*, 39–50.
Pellicciotti, F., S. Ragettli, M. Carenzo, and J. McPhee (2014), Changes of glacier in the Andes of Chile and priorities for future work, *Sci. Total Environ.*, doi:10.1016/j.scitotenv.2013.10.055, in press.
Pepin, N., and M. Losleben (2002), Climate change in the Colorado Rocky Mountains: Free air versus surface temperature trends, *Int. J. Climatol.*, *22*(3), 311–329, doi:10.1002/joc.740.
Petersen, L., and F. Pellicciotti (2011), Spatial and temporal variability of air temperature on a melting glacier: Atmospheric controls, extrapolation methods and their effect on melt modeling, Juncal Norte Glacier, Chile, *J. Geophys. Res.*, *116*, D23109, doi:10.1029/2011JD015842.
Ragettli, S., and F. Pellicciotti (2012), Calibration of a physically based, spatially distributed hydrological model in a glacierized basin: On the use of knowledge from glaciometeorological processes to constrain model parameters, *Water Resour. Res.*, *48*, W03509, doi:10.1029/2011WR010559.
Ragettli, S., and F. Pellicciotti (2013), A framework for the application of physically-oriented glacio-hydrological models in the Himalaya-Karakorum region based on a new approach of uncertainty evaluation, *AGU,* Fall Meet., Abstract C11A-0639.
Ragettli, S., F. Pellicciotti, R. Bordoy, and W. W. Immerzeel (2013a), Sources of uncertainty in modeling the glacio-hydrological response of a Karakoram watershed to climate change, *Water Resour. Res.*, *49*, 1–19, doi:10.1002/wrcr.20450.
Ragettli, S., G. Cortés, J. McPhee, and F. Pellicciotti (2013b), An evaluation of approaches for modelling hydrological processes in high-elevation, glacierized Andean watersheds, *Hydrol. Process*, doi:10.1002/hyp.10055.
Seko, K. (1987), Seasonal variation of altitudinal dependence of precipitation in Langtang Valley, Nepal Himalayas, *Bull. Glacier Res.*, *5*, 41–47.
Shiraiwa, T., K. Ueno, and T. Yamada (1992), Distribution of mass input on glaciers in the Langtang Valley, Nepal Himalayas, *Bull. Glacier Res.*, *10*, 21–30.
Steinegger, U., L. N. Braun, G. Kappenberger, and G. Tartari (1993), Assessment of annual snow accumulation over the past 10 years at high elevations in the Langtang Region, *IAHS Publ. 218*, pp. 155–166, Int. Assoc. of Hydrol. Sci., Wallingford, U. K.
Sugiyama, S., K. Fukui, K. Fujita, K. Tone, and S. Yamaguchi (2013), Changes in ice thickness and flow velocity of Yala Glacier, Langtang Himal, Nepal, from 1982 to 2009, *Ann. Glaciol.*, *54*(64), 157–162, doi:10.3189/2013AoG64A111.
Tahir, A. A., P. Chevallier, Y. Arnaud, L. Neppel, and B. Ahmad (2011), Modeling snowmelt-runoff under climate scenarios in the Hunza River basin, Karakoram Range, Northern Pakistan, *J. Hydrol.*, *409*, 140–117.
Takahashi, S., H. Motoyama, K. Kawashima, Y. Morinaga, K. Seko, H. Iida, H. Kubota, and N. R. Turadahr (1987), Meteorological features in Langtang Valley, Nepal Himalayas, 1985–1986, *Bull. Glacier Res.*, *5*, 35–40.
Ueno, K., and T. Yamada (1990), Diurnal variation of precipitation in Langtang valley, Nepal Himalayas, *Bull. Glacier Res.*, *8*, 93–101.
Viviroli, D., et al. (2011), Climate change and mountain water resources: Overview and recommendations for research, management and policy, *Hydrol. Earth Syst. Sci.*, *15*(2), 471–504, doi:10.5194/hess-15-471-2011.
Yatagai, A., N. Yasutomi, A. Hamada, A. Kitoh, K. Kamiguchi, and O. Arakawa (2012), APHRODITE: Constructing a long-term daily gridded precipitation dataset for Asia based on a dense network of rain gauges, *Bull. Am. Meteorol. Soc.*, *93*(9), 1401–1415.